

Contribution to the supersolid JLTP special issue SS2012

Classification of a supersolid: Trial wavefunctions, Symmetry breakings and Excitation spectra

Yu Chen ¹, Jinwu Ye^{2,3} and Quang Shan Tian ¹

¹*Department of Physics, Peking University, Beijing 100871, China*

² *Department of Physics and Astronomy, Mississippi State University, P. O. Box 5167, Mississippi State, MS, 39762*

³ *Department of Physics, Capital Normal University, Beijing, 100048 China*

(Dated: April 19, 2018)

A state of matter is characterized by its symmetry breaking and elementary excitations. A supersolid is a state which breaks both translational symmetry and internal $U(1)$ symmetry. Here, we review some past and recent works in phenomenological Ginsburg-Landau theories, ground state trial wavefunctions and microscopic numerical calculations. We also write down a new effective supersolid Hamiltonian on a lattice. The eigenstates of the Hamiltonian contains both the ground state wavefunction and all the excited states (supersolidon) wavefunctions. We contrast various kinds of supersolids in both continuous systems and on lattices, both condensed matter and cold atom systems. We provide additional new insights in studying their order parameters, symmetry breaking patterns, the excitation spectra and detection methods.

I. INTRODUCTION

A solid can not flow. It breaks a continuous translational symmetry into a discrete lattice translational symmetry. There are low energy lattice phonon excitations in the solid. While a superfluid can flow even through narrowest channels without any resistance. It breaks a global $U(1)$ symmetry and has the off-diagonal long range order (ODLRO). There are low energy superfluid phonon excitations in the superfluid. A supersolid is a state which breaks both the continuous translational symmetry and the global $U(1)$ symmetry, therefore has both the crystalline order and the ODLRO. The possibility of a supersolid phase in 4He was theoretically speculated in 1970^{1,2}. If so, under the slow rotation of a container, the superfluid component can not rotate, therefore reduces the rotational moment of inertial. This reduction is called Non-Classical Rotational Inertia (NCRI)³. Over the last 40 years, a number of experiments have been designed to search for the supersolid state. Most notably, by using torsional oscillator measurements, the group led by Chan observed a marked $1 \sim 2\%$ NCRI of solid 4He at $\sim 0.2K$ in bulk 4He ⁴. The authors suggested that the supersolid state of 4He maybe responsible for the NCRI. The experiments rekindled extensive both experimental⁵⁻¹¹ and theoretical¹²⁻²⁵ interests. So far, there is still a controversy if a supersolid phase indeed exist in 4He system and is responsible for the NCRI observed in the Chan's experiments. For example, the NCRI experiment in annealed samples⁵ the mass flow experiments^{6,7} and the first principle microscopic calculations¹² indicate that the superfluid effects observed so far in solid He-4 are disordered-induced.

In this manuscript, instead of trying to resolve this controversy, we will discuss some uni-

versal properties of a supersolid such as its ground state wavefunctions, symmetry breakings, elementary excitation spectra and their detections in various possible experimental systems. No matter if supersolid indeed exists in the 4He system or not, it is a new state of matter having its own characteristic behaviors not shared by any other states of matter. Various kinds of supersolids may also be realized in other various bosonic or fermionic, continuous or optical lattice systems.

The rest of the paper is organized as following. In Sect.II, we will discuss the supersolids in continuous 3d and 2d systems. In Sec.II-A, we review the elementary excitation spectrum (called supersolidon) in a possible 3d 4He supersolid with Van der Walls interaction. Sec.II-B is new where we make connections to vacancy supersolid wave functions and derive an effective supersolid Hamiltonian on lattice scales. The supersolidon spectrum discussed in previous works can be extended to the whole Brillouin Zone (BZ). In Sec.II-C, we discuss a possible exciton supersolid with dipole-dipole interaction in a 2d electron-hole bilayer system in some intermediate distances. Sect. III is dedicated to supersolids in lattice systems. We discuss some analogy and also important differences between the continuous supersolids and lattice supersolids. We stress that there is a new kind of supersolid in lattice systems: the valence bond supersolid. In Sect.IV, we study the superfluid density waves. Namely, an inhomogeneous superfluid in a continuous system in IV-A and a Z_2 superfluid density wave inside an optical cavity. In the final Sec.V, we contrast different kinds of supersolids addressed in this paper and also summarize our main results. The possible important effects of disorders will not be discussed in the manuscript and are referred to the original literatures in^{5-7,12,23,25}

II. SUPERSOLIDS IN CONTINUOUS 3 AND 2 DIMENSIONAL SYSTEMS

Classical non-equilibrium hydrodynamics inside a SS was investigated for a long time^{1,16-18}. The classical hydrodynamics will break down at very low temperature where quantum fluctuations dominate. The quantum phenomenological Ginsburg-Landau theories¹⁹⁻²¹ in both 3d and 2d were written down. They can be applied to study possible supersolids in 3 dimensional 4He system and possible exciton supersolids in 2 dimensional electron-hole bilayer systems. The main purposes for the GL theory are (1) It can be used to analyze the stability conditions of a supersolid. As shown in²¹, depending on the parameters of the GL action, the supersolid can be either absent or present in the pressure P versus temperature T phase diagram. The parameters should be determined by microscopic details of the atom-atom interactions. (2) Assuming the supersolid is present in the $P - T$ phase diagram, at the mean field level, the GL theory can be used to determine the lattice structure of a supersolid, (3) When considering fluctuations above the mean field solutions, one may study transitions among different phases using the renormalization group analysis. (4) Well inside a given phase, especially inside a supersolid, one can study the elementary excitations inside such a given phase. The phonon spectrum in a solid or the superfluid phonon (or Goldstone mode) in a superfluid has all been detected by inelastic neutron scattering experiments. So detecting these "supersolidons" by possible inelastic neutron scattering experiments or acoustic attenuation experiments could be smoking gun experiments to confirm a supersolid in any continuous systems. (5) One can study any interacting Bose systems from both path integral quantization and canonical quantization approach. Both approaches are complementary to each other. When combining the effective path integral action inside a supersolid with the known trial vacancy supersolid wavefunctions, one can write down an

effective Hamiltonian on a lattice to gain additional insights to the physical picture of a supersolid. The eigenstates of the Hamiltonian contains both the ground state wavefunction and all the excited states (supersolidon) wavefunctions. The supersolidon spectrum can also be worked out in the whole Brillouin Zone (BZ) including close to the BZ boundary.

Here, we will review the nature of low energy excitations in the SS, namely, focus on the (4) in the above. We refer (1)-(3) to the original papers^{19-21,29}. The part (5) is new and will be discussed in Sect.II-B.

A. Possible supersolid in 3 dimensional 4He with Van der Waals force.

Well inside the SS, the translational symmetry is already broken, so we can parameterize the density deviation order parameter $\delta n(\vec{x}, \tau) = n(\vec{x}, \tau) - n_0$ and the SF complex order parameter $\psi(\vec{x}, \tau)$ as:

$$\begin{aligned}\delta n(\vec{x}, \tau) &= \sum'_{\vec{G}} n_{\vec{G}} e^{i\vec{G}\cdot(\vec{x}+\vec{u}(\vec{x}, \tau))} \\ \psi(\vec{x}, \tau) &= \psi_0(\vec{x}, \tau) [1 \pm \frac{1}{P} \sum'_{\vec{G}} e^{i\vec{G}\cdot(\vec{x}+\vec{u}(\vec{x}, \tau))}]\end{aligned}\quad (1)$$

where the $\psi_0(\vec{x}, \tau) = |\psi_0(\vec{x}, \tau)| e^{i\theta(\vec{x}, \tau)}$ is the SF order parameter, $\vec{u}(\vec{x}, \tau)$ are the 3 lattice phonon modes, the \pm means vacancy-type or interstitial-type supersolids respectively, $n_{\vec{G}}^* = n_{-\vec{G}}$ the " " means the sum over the shortest non-zero reciprocal lattice vector \vec{G} and P is the number of them.

The long wavelength effective action describing the low energy modes inside the SS phase was derived in^{20,21}:

$$\mathcal{L}_{SS} = \frac{1}{2} [\kappa(\partial_\tau \theta)^2 + \rho_{\alpha\beta}^s \partial_\alpha \theta \partial_\beta \theta] + \frac{1}{2} [\rho_n(\partial_\tau u_\alpha)^2 + \lambda_{\alpha\beta\gamma\delta} u_{\alpha\beta} u_{\gamma\delta}] + a_{\alpha\beta} u_{\alpha\beta} i \partial_\tau \theta \quad (2)$$

where κ is the SF compressibility and $\rho_{\alpha\beta}^s$ is the SF stiffness which has the same symmetry as $a_{\alpha\beta}$. The ρ_n is the normal density, the $u_{\alpha\beta} = \frac{1}{2}(\partial_\alpha u_\beta + \partial_\beta u_\alpha)$ is the strain tensor, the $\lambda_{\alpha\beta\gamma\delta}$ is the elastic constant tensor. Obviously, the last term is the crucial *Berry phase* coupling term which couples the lattice phonon modes to the SF mode. The factor of i is important in this coupling. By integration by parts, this term can also be written as $a_{\alpha\beta}(\partial_\tau u_\beta \partial_\alpha \theta + \partial_\tau u_\alpha \partial_\beta \theta)$ which has the clear physical meaning of the coupling between the SF velocity $\partial_\alpha \theta$ and the velocity of the lattice vibration $\partial_\tau u_\beta$. It is this term which makes the low energy modes in the SS to have its own characteristics which could be detected by experiments. The invariance under the Galilean transformation¹⁷ dictates that $a_{\alpha\beta} = \rho_n \delta_{\alpha\beta} - \rho_{\alpha\beta}^s$. Here, we only review the isotropic solid case, the *hcp* lattice and the effects of the topological vortex loop excitations were discussed in the original papers^{20,21}.

A truly isotropic solid can only be realized in a highly poly-crystalline sample. Usual samples are not completely isotropic. However, we expect the simple physics brought about in an isotropic solid may also apply qualitatively to other samples which is very poly-crystalline. For an isotropic solid, $\lambda_{\alpha\beta\gamma\delta} = \lambda \delta_{\alpha\beta} \delta_{\gamma\delta} + \mu(\delta_{\alpha\gamma} \delta_{\beta\delta} + \delta_{\alpha\delta} \delta_{\beta\gamma})$ where λ and μ are Lame coefficients, $\rho_{\alpha\beta}^s = \rho^s \delta_{\alpha\beta}$, $a_{\alpha\beta} = a \delta_{\alpha\beta}$ where $a = \rho_n - \rho_s$. In (\vec{q}, ω_n) space, Eqn.2

becomes:

$$\begin{aligned}\mathcal{L}_{ISS} = & \frac{1}{2}[\rho_n\omega_n^2 + (\lambda + 2\mu)q^2]|u_l(\vec{q}, \omega_n)|^2 + \frac{1}{2}[\kappa\omega_n^2 + \rho_sq^2]|\theta(\vec{q}, \omega_n)|^2 \\ & + aq\omega_n u_l(-\vec{q}, -\omega_n)\theta(\vec{q}, \omega_n) + \frac{1}{2}[\rho_n\omega_n^2 + \mu q^2]|u_t(\vec{q}, \omega_n)|^2\end{aligned}\quad (3)$$

where $u_l(\vec{q}, \omega_n) = iq_i u_i(\vec{q}, \omega_n)/q$ is the longitudinal component, $u_t(\vec{q}, \omega_n) = i\epsilon_{ij}q_i u_j(\vec{q}, \omega_n)/q$ are transverse components of the displacement field. Note that Eqn.3 shows that only longitudinal component couples to the superfluid θ mode, while the two transverse components are unaffected by the superfluid mode. This is expected, because the superfluid mode is a longitudinal density mode itself which does not couple to the transverse modes.

From Eqn.3, we can identify the longitudinal-longitudinal phonon correlation function:

$$\langle u_l u_l \rangle = \frac{\kappa\omega_n^2 + \rho_sq^2}{(\kappa\omega_n^2 + \rho_sq^2)(\rho_n\omega_n^2 + (\lambda + 2\mu)q^2) + a^2q^2\omega_n^2} \quad (4)$$

The $\langle \theta\theta \rangle$ and $\langle u_l\theta \rangle$ correlation functions can be similarly written down. By doing the analytical continuation $i\omega_n \rightarrow \omega + i\delta$, we can identify the two poles of all the correlation functions at $\omega_{\pm}^2 = v_{\pm}^2 q^2$, $q \ll G$ where the two velocities v_{\pm} is given by:

$$v_{\pm}^2 = [\kappa(\lambda + 2\mu) + \rho_s\rho_n + a^2 \pm \sqrt{(\kappa(\lambda + 2\mu) + \rho_s\rho_n + a^2)^2 - 4\kappa\rho_s\rho_n(\lambda + 2\mu)}]/2\kappa\rho_n \quad (5)$$

If setting $a = 0$, then v_{\pm}^2 reduces to the longitudinal phonon velocity $v_{lp}^2 = (\lambda + 2\mu)/\rho_n$ and the superfluid velocity $v_s^2 = \rho_s/\kappa$ respectively. Of course, the transverse phonon velocity $v_{tp}^2 = \mu/\rho_n$ is untouched. For notation simplicity, in the following, we just use v_p for v_{lp} . Inside the SS, due to the very small superfluid density ρ_s , it is expected that $v_p > v_s$. In fact, in isotropic solid He^4 , it was measured that $v_{lp} \sim 450 - 500 m/s$, $v_t \sim 230 \sim 320 m/s$ and $v_s \sim 366 m/s$ near the melting curve⁸. It is easy to show that $v_+ > v_p > v_s > v_-$ and $v_+^2 + v_-^2 > v_p^2 + v_s^2$, but $v_+ v_- = v_p v_s$, so $v_+ + v_- > v_p + v_s$ (see Fig.1). Note that because the Galilean invariance dictates $a = \rho_n - \rho_s$, for $\rho_s \ll \rho_n$, one can see $\rho_s\rho_n + a^2 \gg \rho_s\rho_n$, so v_+ (v_-) are considerably above (below) v_p (v_s), so the two supersolidons, especially the softening of the lower branch, may be easily distinguished by possible neutron scattering experiments.

By doing the analytical continuation $i\omega_n \rightarrow \omega + i\delta$, we can take the imaginary part and find:

$$\begin{aligned}Im\langle u_l u_l \rangle_{i\omega_n \rightarrow \omega + i\delta} = & \frac{v_s^2 - v_+^2}{v_+^2 - v_-^2} \frac{\pi}{2\rho_n v_+ q} \frac{1}{q} [\delta(\omega - v_+ q) - \delta(\omega + v_+ q)] \\ & - \frac{v_s^2 - v_-^2}{v_+^2 - v_-^2} \frac{\pi}{2\rho_n v_- q} \frac{1}{q} [\delta(\omega - v_- q) - \delta(\omega + v_- q)]\end{aligned}\quad (6)$$

It is easy to see that the second term can be achieved from the first term just by $v_+ \leftrightarrow v_-$. Setting $a = 0$, then $v_+ = v_p$, $v_- = v_s$, the second term just vanishes, the first term recovers the excitation spectrum of the lattice phonons. When $a \neq 0$, then Eqn.6 becomes a mixing of the lattice phonons and superfluid phonons, the first and second term give the excitation energies and the two corresponding spectral weights.

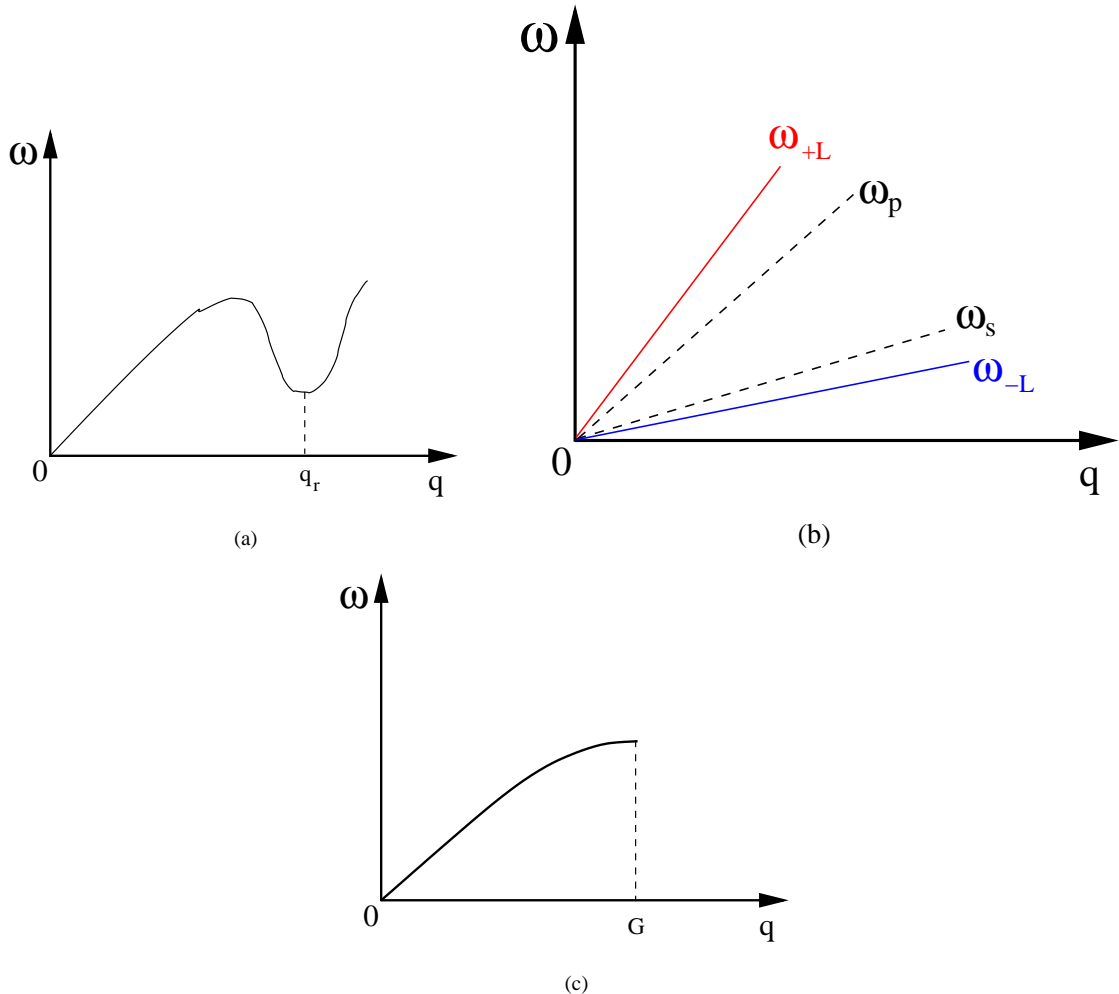


FIG. 1: (Color figure online) The elementary low energy excitations inside a (a) superfluid, the $q_r \sim G$ is the roton minimum position. (b) supersolid (c) solid, the G is the shortest reciprocal lattice vector in the Brillouin Zone (BZ). For simplicity, only excitation spectra in a simplified 3d isotropic solid and 2d triangular lattice were shown. In (b) The coupling between the phonon mode $\omega_p = v_p q$ (the upper dashed line) and the superfluid mode $\omega_s = v_s q$ (the lower dashed line) leads to the two new "supersolidon" modes $\omega_{\pm} = v_{\pm} q$ when $q \ll G$ (solid lines) in the SS. Their corresponding spectral weights are listed in Eqn.6 and 7. These two new supersolid modes and the spectral weights should be detected by in-elastic neutron scatterings²⁷. The dispersion form of the supersolidon near BZ G can be worked out from the effective Hamiltonian at the lattice scale Eqn.12.

Very similarly, we can find

$$\begin{aligned}
 Im\langle\theta\theta\rangle_{i\omega_n \rightarrow \omega+i\delta} = & \frac{v_p^2 - v_+^2}{v_+^2 - v_-^2} \frac{\pi}{2\kappa v_+} \frac{1}{q} [\delta(\omega - v_+ q) - \delta(\omega + v_+ q)] \\
 & - \frac{v_p^2 - v_-^2}{v_+^2 - v_-^2} \frac{\pi}{2\kappa v_-} \frac{1}{q} [\delta(\omega - v_- q) - \delta(\omega + v_- q)]
 \end{aligned} \quad (7)$$

It is easy to see that the second term can be achieved from the first term just by $v_+ \leftrightarrow$

v_- . Setting $a = 0$, then $v_+ = v_p$, $v_- = v_s$, the first term just vanishes, the second term recovers the excitation spectrum of the superfluid phonons. When $a \neq 0$, then Eqn.7 become a mixing of the lattice phonons and superfluid phonons, the first and second term give the excitation energies and the two corresponding spectral weights. So detecting these "supersolidons" in Fig.1b by possible inelastic neutron scattering experiments or acoustic attenuation experiments could be smoking gun experiments to confirm a supersolid in any continuous systems. The experimental implications of the supersolidons on X-ray scatterings, density-density correlation functions, specific heats were discussed in^{20,21}.

However, it is well known that the GL theory is a phenomenological theory. In fact, depending on the parameter regimes in the GL theory in²¹, the author discussed both the non-existence and existence of supersolid, also the vacancy-type and interstitial-type the supersolid if it exists. Into which parameter regime will the 4He fall can only be studied by various numerical calculations^{12,13}. But so far, it seems that most of the numerical simulations with the 4He atoms interacting each other with Van der Waals forces favor a commensurate solid instead of either vacancy-type or interstitial type supersolid. Even so, the supersolid could be a meat-stable phase with sufficiently long life time and lead to some experimental observable signatures within some time scale.

B. Connections with the trial Wavefunctions of a supersolid and an effective Hamiltonian

In this subsection, we contrast wave functions of a conventional solid, a solid with local tunneling process and a supersolid. We also contrast their corresponding effective Hamiltonian.

1. Trial wavefunction for a supersolid and the effective Hamiltonian

A well known trial wavefunction^{2,12,13} for a supersolid in the second quantization form was written in the appendix A of Ref.²¹:

$$|SS, \phi\rangle = \prod_{i=1}^N (\cos \frac{\theta}{2} + \sin \frac{\theta}{2} e^{i\phi} b_i^\dagger) |0\rangle \quad (8)$$

where $\theta \neq \pi$. The average boson number is $M = N \sin^2 \frac{\theta}{2} < N$. The vacancy number is $N_b = N \cos^2 \frac{\theta}{2} > 0$.

A supersolid state $|SS, M\rangle$ with $M < N$ bosons is given by:

$$|SS, M\rangle = \int_0^{2\pi} \frac{d\phi}{2\pi} e^{-iM\phi} |SS, \phi\rangle = (\cos \frac{\theta}{2})^N C_N^M (\tan \frac{\theta}{2})^M \frac{1}{M!} \sum_{i_1, \dots, i_M} b_{i_1}^\dagger \cdots b_{i_M}^\dagger |0\rangle \quad (9)$$

where the total boson number M and the global phase ϕ are two Hermitian conjugate variables satisfying the commutation relation: $[\delta M, \phi] = i\hbar$. It leads to the uncertainty relation $\Delta M \Delta \phi \geq 1$.

Following the procedures in²⁶ to derive the first quantization form of a wavefunction from its second quantized form in the exciton superfluid in bilayer quantum Hall systems, one can find the first quantization form of the supersolid wavefunction:

$$|SS, M\rangle = C \sum_P \mathcal{S} \left[\prod_{i=1}^{M < N} \phi(\vec{r}_i - \vec{R}_{P_i}) \right] \quad (10)$$

where the P is the sum over all the C_N^M possible ways of selecting $M < N$ sites from the N sites. The \mathcal{S} is the symmetrization acting on the boson coordinates \vec{r}_i . The C is the normalization constant.

In order to consider the mutual interaction between atoms in neighboring sites, it is necessary to incorporate the Jastrow factor² into the above wave function:

$$|SS, M\rangle_J = C \sum_P \mathcal{S} \left[\prod_{i=1}^{M < N} \phi(\vec{r}_i - \vec{R}_{P_i}) \prod_{i < j} J(r_{ij}) \right] \quad (11)$$

where the $\prod_{i < j} J(r_{ij}) = e^{-\sum_{i < j} u(r_{ij})}$ is the Jastrow factor, the $u(r_{ij})$ is the Lennard-Jones 6-12 potential with a hard core repulsion.

When comparing the effective action Eqn.2 with the ground state wavefunction Eqn.8, one can see that the angle θ corresponds to the superfluid density fluctuation, while the angle ϕ is the most important phase fluctuations in Eqn.2. The phonon modes in 2 corresponds to $\vec{r}_i \rightarrow \vec{R}_i + \vec{u}(\vec{R}_i)$ in Eqn.11. In fact, as argued in the following, the trial wavefunction Eqn.11 can be taken as the exact ground state of the effective Hamiltonian Eqn.12.

Motivated by the one to one correspondence between the effective action Eqn.2 and the ground state wavefunctions Eqn.11, one can write the corresponding effective Hamiltonian on a lattice scale:

$$\begin{aligned} \mathcal{H}_{SS} = & \sum_{\vec{R} \in M < N} \frac{P^2(\vec{R})}{2M} + \frac{1}{2} \sum_{\alpha, \beta, \vec{R}, \vec{R}'} u_\alpha(\vec{R}) D_{\alpha\beta}(\vec{R} - \vec{R}') u_\alpha(\vec{R}') \\ & + \frac{1}{2} \delta\rho(-\vec{q}) V(\vec{q}) \delta\rho(\vec{q}) + \frac{1}{2} \rho_{\alpha\beta}^s \partial_\alpha \theta \partial_\beta \theta + a_{\alpha, \beta} (\Delta_\alpha u_\beta + \Delta_\beta u_\alpha) \delta\rho \end{aligned} \quad (12)$$

where the sum over $\vec{R} \in M < N$ is only over the $M < N$ sites where the atoms occupy, the vacancy number $b^\dagger b = N - M$ flow through the whole lattice and condense into the superfluid state. The SF compressibility $\kappa^{-1} = \lim_{q \rightarrow 0} V(\vec{q})$ where the form $V(q) = a - bq^2 + cq^4$, $a, b, c > 0$ ²¹ is needed to lead to the superfluid mode in Fig 1a in the whole BZ. The u_α, P_β and the $\theta, \delta\rho$ are the two sets of conjugate variables satisfying $[u_\alpha(\vec{R}), P_\beta(\vec{R}')] = i\hbar \delta_{\alpha, \beta} \delta_{\vec{R}, \vec{R}'}$ and $[\theta, \delta\rho] = i\hbar$. When the vacancies b are moving through the whole lattice²⁸, the superfluid density fluctuation couples to the lattice vibration through the last term where $\Delta_\alpha u_\beta = u_\beta(\vec{R} + \hat{e}_\alpha) - u_\beta(\vec{R})$ is the lattice difference.

Obviously, the long wavelength limit of Eqn. 12 leads to Eqn.2. The effective Hamiltonian also hold on lattice scales. When neglecting the vortex excitations, the Eqn.12 is quadratic, the standard Bogoliubov transformation can be used to extend the supersolidon dispersion relation in Fig.1b to the whole BZ zone including near to the BZ boundary G in the Fig 1c. The vortex excitations inside a supersolid were discussed in²¹.

For comparisons, in the following, we also write down the wavefunction and the corresponding effective Hamiltonian of a conventional solid and a quantum solid with local quantum tunneling and exchange process.

2. Wavefunction for a conventional solid and the effective Hamiltonian

For a conventional solid, one atom is attached to a given lattice site. Because all the atoms can be treated as distinguishable as labeled by its attached site i , so the symmetrization operator \mathcal{S} in Eqn.11 is not necessary.

$$|Solid\rangle = \prod_{i=1}^M \phi(\vec{r}_i - \vec{R}_i) \prod_{i < j} J(r_{ij}) \quad (13)$$

Obviously, its effective Hamiltonian is just the first line in the Eqn.12.

$$\mathcal{H}_{Solid} = \sum_{\vec{R} \in M < N} \frac{P^2(\vec{R})}{2M} + \frac{1}{2} \sum_{\alpha, \beta, \vec{R}, \vec{R}'} u_\alpha(\vec{R}) D_{\alpha\beta}(\vec{R} - \vec{R}') u_\alpha(\vec{R}') \quad (14)$$

whose phonon spectrum has been discussed in textbooks

3. Wavefunction for a commensurate solid with local tunnelings and its effective Hamiltonian

In a commensurate solid, the number of atoms is equal to the number of sites $M = N$. There exist still local quantum tunneling and exchange processes. But these local quantum tunneling and exchange process will not lead to a global phase coherence. Due to these local tunneling processes, the atoms still need to be treated as in-distinguishable identical particles, so the the symmetrization operator \mathcal{S} in Eqn.11 is still necessary, the wavefunction can be written as

$$|Solid\rangle_{le} = \mathcal{S} \left[\prod_{i=1}^{M=N} \phi(\vec{r}_i - \vec{R}_{P_i}) \prod_{i < j} J(r_{ij}) \right] \quad (15)$$

where the le means local exchange processes. The corresponding Hamiltonian is

$$\begin{aligned} \mathcal{H}_{solid+le} = & \sum_{\vec{R} \in M < N} \frac{P^2(\vec{R})}{2M} + \frac{1}{2} \sum_{\alpha, \beta, \vec{R}, \vec{R}'} u_\alpha(\vec{R}) D_{\alpha\beta}(\vec{R} - \vec{R}') u_\alpha(\vec{R}') \\ & - \frac{\hbar^2}{2m} \psi^\dagger \nabla^2 \psi + \mu \psi^\dagger \psi + u(\psi^\dagger \psi)^2 + a_{\alpha, \beta} (\Delta_\alpha u_\beta + \Delta_\beta u_\alpha) \psi^\dagger \psi \end{aligned} \quad (16)$$

where the u_α, P_β and the ψ, ψ^\dagger are the two sets of conjugate variables satisfying $[u_\alpha(\vec{R}), P_\beta(\vec{R}')] = i\hbar \delta_{\alpha, \beta} \delta_{\vec{R}, \vec{R}'}$ and $[\psi(\vec{x}), \psi^\dagger(\vec{x}')] = i\hbar \delta(\vec{x} - \vec{x}')$. The local tunneling mode couples to the lattice vibration through the last term. Due to the positive mass term $\mu > 0$, the local mode has a gap, so integrating out the gapped mode ψ will lead to the same effective Hamiltonian Eqn.14 as the conventional solid. So the lattice phonon mode will not be affected by the gapped bulk normal fluid mode.

C. Possible 2 dimensional Exciton supersolid in electron-hole bilayer with dipole-dipole interaction.

In this subsection, we will discuss another bosonic system with much longer range dipole-dipole interactions: excitons in electron-hole semi-conductor bilayer (EHBL) systems²⁹. We will argue that due to the special form of dipole-dipole interaction, this system may have a better chance to realize a supersolid in some parameter regime. There are also some numerical evidences to support such a claim⁴⁷. Indeed, as shown in²¹ and briefly mentioned at the beginning of Sect.I, depending on the parameters of the GL action, the supersolid can be either absent or present in the pressure P versus temperature T phase diagram. The parameters, in turn, are determined by microscopic details of the atom-atom interactions.

In the last decade, degenerate exciton systems have been produced by different experimental groups with different methods in quasi-two-dimensional semiconductor *GaAs/AlGaAs* coupled quantum wells structure²⁹. There are two important dimensionless parameters in the EHBL. (1) One is the dimensionless distance $\gamma = d/a_{ex}$ between the two layers.

The $a_{ex} = \hbar^2\epsilon/e^2m_r = \epsilon \frac{m_0}{m_r} a_B \sim 100a_B \sim 50\text{\AA}$ is the size of an exciton, the m_0 is the electron bare mass and $1/m_r = 1/m_e + 1/m_h$ is the reduced mass of the excitons and $a_B = \hbar^2/e^2m_0 \sim 0.53\text{\AA}$ is the bare Bohr radius. The binding energy of an exciton is $E_b = -e^2/2a_{ex}\epsilon = -\frac{m_r}{m_0} \frac{1}{\epsilon^2} \frac{e^2}{2a_B} \sim -10\text{meV}$. (2) Another is r_s . The $r_s a_{ex}$, defined by $\pi(r_s a_{ex})^2 n = 1$, is the typical interparticle distance in a single layer. The r_s is the ratio of the potential energy over kinetic energy in a single layer. It is easy to see that the ratio of intralayer Coulomb V_{11} over the interlayer Coulomb V_{12} interaction is given by $\alpha = V_{11}/V_{12} = d/r_s a_{ex}$. So when the interlayer Coulomb interaction dominates $\alpha < 1$, the EHBL is expected to exhibit the superfluid of excitons. If the density of excitons is sufficiently low (large r_s), then the system is in a weakly coupled Wigner solid state at very large distance and become an BEC excitonic superfluid (ESF) at short distance. In the following, we argue²⁹ that there could be an exciton supersolid (ESS) phase intervening between the ESF and Wigner solid phase, as the system evolves from the BEC ESF to the weakly coupled Wigner solid when the distance increases. The argument relies heavily on the dipole-dipole interaction between the excitons.

If we assume an exciton is already formed at relatively short interlayer distance, its kinetic energy $K \sim \frac{\hbar^2}{M(r_s a_{ex})^2}$ where $M = m_e + m_h$ is the total mass of an exciton. Due to the dipole-dipole interactions between the excitons, its potential energy $P \sim \frac{e^2 d^2}{\epsilon (r_s a_{ex})^3}$. When $K < P$, namely, $\sqrt{m_r/M} \sqrt{r_s} < d/a_{ex}$, the EHBL could favor a excitonic (or dipolar) normal solid (ENS) state. As argued above, when $d/a_{ex} < r_s$, the EHBL is in a ESF state. So in the intermediate distance $\sqrt{r_s}/2 < d/a_{ex} < r_s$ where we used $M/m_r \sim 5$, the system may favor a excitonic (or dipolar) supersolid (ESS) state. When $d/a_{ex} > r_s$, it will become the excitonic normal solid (ENS) due to the long range dipole-dipole $1/r^3$ repulsive interactions. For the present experimental density regime²⁹ $n \sim 10^{10}\text{cm}^{-2}$, $r_s \sim 20$, so the excitons are tightly bound pairs in real space. In this $r_s \sim 20 \gg 1$ limit, there is a broad distance regime $2 < d/a_{ex} < 20$ where the system could be in the ESS state. As the distance increases to the critical distance $d > d_{c1}$, the roton minimum in the Fig.1a may drive the instability of the ESF to a formation of a solid. Because the lattice constant $r_s a_{ex}$ of the resulting solid is completely fixed by the parameter r_s which is independent of the distance, so the resulting solid is likely to have vacancies with density $n_v(0)$ even at $T = 0$. By contrast, in solid Helium 4, the density is self-determined by the pressure $n = \frac{\partial P}{\partial \mu}|_{T,V}$, so the density and pressure go hand in hand, the solid ${}^4\text{He}$ is likely to be commensurate. We expect that the vacancy-vacancy interaction is also a repulsive dipole-dipole one. The condensation of these repulsively interacting vacancies at $T = 0$ leads to the SF mode inside the in-commensurate ENS. This resulting state is the ESS state with a lattice constant slightly smaller than $r_s a_{ex}$ to accommodate the extra vacancies. As the distance increases to $d > d_{c2} > d_{c1}$, $n_v(0) = 0$, the resulting state is a commensurate ENS whose lattice constant is locked at $r_s a_{ex}$. As distance increases further, the ENS will crossover to the two weakly coupled Wigner crystal. It becomes feasible to experimentally explore all the possible phases and phase transitions in the EHBL in the near future.

From the mean field analysis of the Ginsburg-Landau action in²⁹, the lattice structure of the excitonic supersolid should be a triangular lattice. When studying the excitations spectrum inside the ESS, a similar GL action can be constructed as its 3 dimensional counter part²⁹. For a triangular lattice, $\lambda_{\alpha\beta\gamma\delta} = \lambda\delta_{\alpha\beta}\delta_{\gamma\delta} + \mu(\delta_{\alpha\gamma}\delta_{\beta\delta} + \delta_{\alpha\delta}\delta_{\beta\gamma})$ where λ and ν are Lame coefficients, $\rho_{\alpha,\beta}^s = \rho^s \delta_{\alpha,\beta}$, $a_{\alpha,\beta} = a \delta_{\alpha,\beta}$. Eqn.3, the following equations an Fig.1 apply. Note that the isotropic 3d solid discussed in Sec.II-1 is just a simplification. The supersolidons in

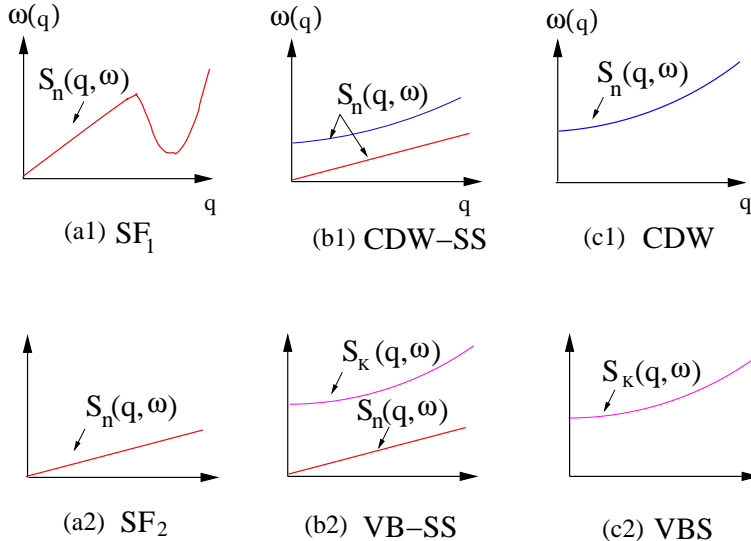


FIG. 2: (Color figure online) The excitation spectra in the CDW, VBS, SF, CDW-SS and VB-SS states in a lattice. They correspond to the peak positions of the corresponding dynamic response functions shown with arrows⁵⁰. In the (b1) and (c1) cases, the starting wavevector is \vec{Q}_n in the upper CDW branch. In the (b2) and (c2) cases, the starting wavevector is \vec{Q}_K in the upper VBS branch. The corresponding spectral weights are worked out in⁵⁰.

3d hcp crystal were discussed in²⁰. While Eqn.3 holds rigorously for a 2d triangular lattice. The differences between 3d and 2d cases were discussed in²⁹.

III. DENSITY WAVE SUPERSOLIDS AND VALENCE BOND SUPERSOLID IN LATTICE SYSTEMS

The extended boson Hubbard model (EBHM) with various kinds of interactions, on all kinds of lattices and at different filling factors is described by the following Hamiltonian:

$$\begin{aligned}
 H_{EBHM} = & -t \sum_{\langle ij \rangle} (b_i^\dagger b_j + h.c.) - \mu \sum_i n_i + \frac{U}{2} \sum_i n_i(n_i - 1) \\
 & + V_1 \sum_{\langle ij \rangle} n_i n_j + V_2 \sum_{\langle\langle ik \rangle\rangle} n_i n_k + \dots
 \end{aligned} \tag{17}$$

where $n_i = b_i^\dagger b_i$ is the boson density, t is the nearest neighbor hopping amplitude. U, V_1, V_2 are onsite, nearest neighbor (nn) and next nearest neighbor (nnn) interactions respectively, the \dots may include further neighbor interactions, dipole-dipole interaction $V_d = \frac{p^2}{|\vec{r}_i - \vec{r}_j|^3}$ and possible ring-exchange interactions. A supersolid in Eqn.17 is defined as the simultaneous orderings of ferromagnet in the XY component (namely, $\langle b_i \rangle \neq 0$) and CDW in the Z component. The EBHM, especially the stability of the supersolid phase has been studied by spin wave expansion³⁷, the Quantum Monte-Carlo (QMC) simulations³⁸⁻⁴³ and the dual vortex method (DVM)³⁰⁻³⁴ which is a Ginsburg-Landau (GL) action in the dual vortex picture.

A. The Dual Ginsburg-Landau approach: the dual vortex method to study supersolids in lattices

In³², based on the dual vortex degree of freedoms³⁰, the author developed a systematic dual Ginsburg-Landau (GL) action to study all the possible phases and phase transitions in the EBHM Eqn.17 in bipartite lattices such as a honeycomb and square lattice near half filling. The dual GL theory can be used to derive the symmetry breaking patterns of various insulating and supersolid states, the transitions among different phases and excitation spectrum in a given insulating phase, especially in various kinds of supersolids. In the insulating side, it was found that there are two consecutive transitions at zero temperature driven by the chemical potential: in the Ising limit, a Commensurate-Charge Density Wave (CDW) at half filling to a narrow window of CDW supersolid (CDW-SS), then to an Incommensurate-CDW ; in the easy-plane limit, a Commensurate-Valence Bond Solid (VBS) at half filling to a narrow window of VBS supersolid (VBS-SS), then to an Incommensurate-VBS. The first transition is second order in the same universality class as the Mott to insulator transition, therefore has the exact critical exponents $z = 2, \nu = 1/2, \eta = 0$ with logarithmic corrections³⁶, while the second one is first order. The VBS-SS is a new kind of solid which only happens on a lattice, so no analog in a continuous system discussed in the Sec.II. The VBS-SS maybe stabilized in the presence of ring-exchange terms³⁵. The excitation spectra in these phases are shown in the Fig.2. The transition from the the SF to the CDW-SS transition is driven by the condensation of diagonal vortex-antivortex pair without the condensations of the individual vortex³⁶. In the direct boson picture, it may correspond to the gap closing at the roton minimum. The transition from the the SF to the VBS-SS transition is driven by the condensation of off-diagonal vortex-antivortex pair without the condensations of the individual vortex. Unfortunately, it is still not clear what kind of physical processes it corresponds to in the direct boson picture³⁶. Very recently, the author in^{33,34} also studied various kinds of supersolids in frustrated lattices such as triangular and Kagome lattices . As first discovered in³⁷, a CDW supersolid is very robust in a triangular lattice slightly away the 1/3 filling. It could be either vacancy-like or interstitial-like supersolid. But there is no VBS-SS which was discovered in bi-partite lattices. There could also be a CDW-VS supersolid which has the three kinds of orders: CDW-order, VB order and the superfluid order. In a Kagome lattice, there is no VBS-SS either, but there could be CDW-SS and the CDW-VB-SS. So the VBS-SS is unique to bi-partite lattices, while the CDW-VB-SS is unique to frustrated lattices. While, the CDW-SS can happen in both bi-partite and frustrated lattices.

Just like the GL approach to the possible supersolids in continuous systems discussed in Sec.I, the DVM developed in³⁰⁻³⁴ is a symmetry-based approach which, in principle, can be used to classify all the possible phases, especially supersolid phases, and phase transitions. But if a particular phase identified by the DVM will become a stable ground state or not depends on the specific competitions among all the possible parameters in the EBHM in Eqn.17. This kind of question can only be addressed by a microscopic approach such as Quantum Monte-Carlo (QMC) simulations on a specific Hamiltonian. In the following, we just compare with QMC simulations in V_1, V_2 models and the dipole-dipole interaction model $V_d = \frac{p^2}{|\vec{r}_i - \vec{r}_j|^3}$.

B. Quantum Monte-Carlo simulations in lattice models

Due to the lack of sign problems in the EBHM Eqn.17, Numerical calculations such as Quantum Monte-carlo simulations are very successful in studying the EBHM with various kinds of long range interactions. The combinations of the DVM discussed in the last subsection and the QMC simulations to be discussed in this subsection lead to converging pictures of various supersolids in lattice systems.

1. QMC simulations in lattices with V_1, V_2 interactions

There have been extensive QMC on the EBHM Eqn.17, to especially search for stable supersolid phases in various bipartite and frustrated lattices³⁸⁻⁴³. For hard core bosons in a square lattice, it was shown by the QMC in³⁸ that the (π, π) X-CDW SS slightly away from 1/2 filling is not stable against phase separation with $U = \infty, V_1 > 0, V_2 = 0$, but the $(\pi, 0)$ stripe SS is indeed stable with $U = \infty, V_1 = 0, V_2 > 0$. The transition from the stripe SS to the SF is a first order transition³⁶. For soft core bosons with $U < \infty, V_1 > 0, V_2 = 0$, the interstitial-like supersolid slightly above 1/2 filling is stable, although the vacancy-like supersolid slightly below 1/2 filling is still unstable against phase separation³⁹. Similar phenomena were also found for soft core bosons in a honeycomb lattice near half fillings⁴⁰. The claim that the CDW to the CDW-SS transition at $d = 2$ driven by the chemical potential is in the same universality class of SF to Mott transition with the critical exponents $z = 2, \nu = 1/2, \eta = 0$ reached from the DVM³² was indeed confirmed by the QMC in⁴¹. Possible supersolids were also studied in a $d = 1$ lattice⁴¹. At $d = 1$, the SF to the CDW transition is in the Kosterlitz-Thouless (KT) transition universality class instead of the first order transition in $d = 2$ and $d = 3$. We expect that the SF to the CDW-SS transition at $d = 1$ is also in the KT transition universality class. The QMC simulations in a triangular lattice⁴² found stable supersolids near 1/3 filling even for hard core bosons with $U = \infty, V_1 > 0$, as first predicted by the spin wave expansion in³⁷. However, for hard core bosons with $U = \infty, V_1 > 0$, no stable supersolids were found near 1/3 fillings in a Kagome lattice⁴³. But we do expect^{33,34} that a CDW-VB supersolid should be stable in a soft core boson case with $U < \infty, V_1 > 0$. Furthermore, a stripe supersolid should be stable even in a hard core case with $U = \infty, V_1 > 0, V_2 > 0$.

2. QMC simulations in optical lattices with Dipolar bosons

Since the experimental realization of polar fermionic molecules⁴⁴⁻⁴⁰ $K + ^{87}Rb$, there have been extensive research activities to study new states of matter which can be formed by these polar molecules⁴⁵⁻⁴⁷. Stable bosonic molecules $^{39}K + ^{87}Rb$ should also be within experimental reach in the near future. The particular feature of these polar molecules are that they carry large electric dipole moments, therefore interact with each other via long-rang anisotropic dipole-dipole interactions similar to excitons in the EHBL in Sec.II-2. It was argued in Sect.II-2 that the dipole-dipole interaction between indirect excitons may favor a formation of vacancy-like exciton supersolid in some intermediate distances between the bilayers. Here, there are extensive numerical evidences that the dipole-dipole long-range interaction is especially favorable to the formation of the CDW supersolid⁴⁵⁻⁴⁷. Although the QMC simulations in³⁸ found that for hard-core bosons in a square lattice with the $V_1 > 0$ interaction, the X-CDW is not stable against a phase separation slightly away from 1/2 filling, the QMC simulations in⁴⁵ found that for hard core bosons with the dipole-dipole interaction, the X-CDW is stable in a large parameter regime slightly away from 1/2 fillings. Furthermore, it was found the CDW-SS to the SF transition is a second order transition in the $3d$ Ising universality class³⁶, instead of a first order transition in the $V_1 > 0$ case³⁸. Very

similarly, the $\vec{Q}_n = 2\pi/3(1,1)$ X-CDW supersolid were found to be stable in a large parameter regimes near the 1/3 filling in a triangular lattice⁴⁶. Stable supersolid phase was also identified in dipolar bilayer systems⁴⁷. In fact, the ^{52}Cr atoms⁴⁸ carry exceptionally large magnetic dipole moment and therefore interact with each other also with the anisotropic long-range dipole-dipole interaction. All kinds of CDW and CDW supersolids could be very likely realized in near future experiments with either dipolar bosons or ^{52}Cr atoms loaded in square and triangular lattices.

C. Detection of supersolids and their excitations in optical lattices

There could be many kinds of detection methods of possible supersolids in continuous systems such as the NCRI^{4,5}, mass flow^{6,7}, melting curve⁸, acoustic attenuation⁹, specific heat¹⁰ and X-ray scattering. So far, the detection methods of the possible charge neutral cold atoms loaded in optical lattices are very limited. However, in recent works^{49,50}, the authors developed a systematic and unified theory of using the optical Bragg scattering, atomic Bragg scattering or cavity QED to detect the ground state and the excitation spectrum of many quantum phases of interacting bosons loaded in bipartite and frustrated optical lattices. They showed that the two photon Raman transition processes in the three detection methods not only couple to the density order parameter, but also the *valence bond order* parameter due to the hopping of the bosons on the lattice. This valence bond order coupling is very sensitive to any superfluid order or any Valence bond (VB) order in the quantum phases to be probed. These quantum phases include not only the well known superfluid and Mott insulating phases, but also other important phases such as various kinds of charge density waves (CDW), valence bond solids (VBS), CDW-VBS phases with both CDW and VBS orders unique to frustrated lattices, and also various kinds of supersolids. So if the supersolids of dipolar bosons or ^{52}Cr atoms can indeed be realized in optical lattice, the light scattering methods discussed in^{49,50} could be used to detect their existence and excitation spectra shown in Fig.2.

IV. SUPERFLUID DENSITY WAVE (SFDW)

As stressed in the previous two sections, for supersolids in both continuous and lattice systems, there are always a underlying normal solid components δn in Eqn.1. So in continuous system, there must be vacancies in an in-commensurate solid flowing through the whole lattice to form a supersolid. While on lattices, there must be vacancies or interstitials away from commensurate fillings to stabilize a lattice supersolid. In this section, we discuss Superfluid density wave (SFDW) which has no such underlying normal solid components δn . Its lattice structure is completely due to the modulations of the order parameter ψ in Eqn.1 itself. So SFDW can happen at any filling factors.

A. SFDW in continuous systems

So far, we only discussed possible supersolids and their excitation spectra in bosonic systems. In fact, there is also an analog in fermionic systems which is the well known, but putative Larkin-Ovchinnikov-Fulde-Ferrell (LOFF) pairing state^{51,52}. When the number of

spin up electron is equal to the number of down spin electron $n_\uparrow = n_\downarrow$, then the pairing between them is at $\vec{k} = 0$ only. If there is a mismatch $\delta n = n_\uparrow - n_\downarrow$, then pairing may shift to a non-zero momentum $q_0 \sim k_{F\uparrow} - k_{F\downarrow}$ which is the FFLO pairing state. By using the GL theory near the transition from the normal to the FFLO state, at a mean field level, the authors in⁵³ constructed the GL free energy in the momentum space in terms of the S-wave pairing order parameter $\psi_{FFLO}(\vec{x}) = \langle c_\uparrow^\dagger(\vec{x})c_\downarrow(\vec{x}) \rangle$:

$$F_{FFLO} = \sum_G \frac{1}{2} r_G |\psi_G|^2 + u \sum_G \psi_{G_1} \psi_{G_2} \psi_{G_3} \psi_{G_4} \delta_{G_1+G_2+G_3+G_4} \\ + v \sum_G \psi_{G_1} \psi_{G_2} \psi_{G_3} \psi_{G_4} \psi_{G_5} \psi_{G_6} \delta_{G_1+G_2+G_3+G_4+G_5+G_6} \quad (18)$$

where $r_G = T - T_c$ and u, v are the fourth and sixth order interaction terms respectively. This equation should be understood as an expansion in terms of the FFLO order parameter ψ_G , not as a gradient expansion anymore. The GL action was used to understand the lattice structure of the FFLO state. If $r_G > 0$, the system is in the normal state with $\langle \psi(\vec{G}) \rangle = 0$, while when $r_G < 0$, it is in the FFLO phase with the order parameter: $\langle \psi(x) \rangle = \sum_{i=1}^P \Delta_i e^{i\vec{G}_i \cdot \vec{x}}$, $|\vec{G}_i| = q_0$. From Eqn.18, the authors found the most favorable lattice structures of the FFLO state is the stripe state (LO state with $P = 2$) in large number of parameter regimes. The FFLO state maybe considered as a weak coupling (or fermionic) analog of the (bosonic) supersolid.

So far all the previous analysis in a FFLO state⁵¹⁻⁵³ are only at a mean field level. Just from symmetry breaking point of views, the FFLO state breaks both $U(1)$ symmetry and the translational symmetry, therefore it also supports two kinds of Goldstone modes. (1) The Goldstone mode due to the $U(1)$ symmetry breaking. (2) the lattice phonon modes due to the translational symmetry breaking. Above the mean field solution, very similar to the second equation in Eqn.1, the pairing order parameter can be written as:

$$\psi_{FFLO}(\vec{x}, \tau) = \Delta e^{i\theta(\vec{x}, \tau)} \sum'_{\vec{G}} e^{i\vec{G} \cdot (\vec{x} + \vec{u}(\vec{x}, \tau))} \quad (19)$$

where $\theta(\vec{x}, \tau)$ and $\vec{u}(\vec{x}, \tau)$ are the superfluid phonon and the lattice phonon modes respectively. The LO state corresponds to $P = 2$. For a charged condensed matter system such as a electron system, due to the Higgs mechanism, the Goldstone mode $\theta(\vec{x}, \tau)$ will be just eaten by the gauge field. However, for a neutral system such as the pairing between two species of fermions with unequal populations in cold atom systems across a Feshbach resonance, the Goldstone mode $\theta(\vec{x}, \tau)$ survives. The coupling between the two phonon modes in Eqn.19 are also described by a equation similar to Eqn.3. The only difference is that the lattice structure is a LO state instead of an isotropic solid. After taking this difference into account, the elementary excitations inside the FF state are similar to those in the Fig.1b and the corresponding spectral weights can be worked out similarly. The experimental signatures of the elementary excitations can also be worked out similarly. Unfortunately, so far, there is still no convincing evidences for a FFLO state in either condensed matter or cold atom systems yet.

B. SFDW inside an optical cavity

As shown in Sec.III, various kinds supersolids may be stabilized in the presence of long-range interactions. In this section, we discuss a superfluid density wave (SFDW) of bosons where the long range interactions between bosons are mediated by cavity photons. The experimental set-up is shown in Fig.3a where cold atoms such as ^{87}Rb are embedded in a high finesse standing wave cavity and are strongly interacting with cavity photons, subject to a transverse pumping. There are two kinds of complementary measurements. One is the probe shown in Fig.3a which detects the Floorescence spectrum of small cavity leaking photons^{54,55}. Another is the absorption imaging which detects the atomic distribution inside the cavity. In a frame rotating with the pumping frequency ω_p in the Fig.3a, the experimental set-up in Fig.3a can be mapped to the Z_2 Dicke model⁵⁶ Eqn.20:

$$H_{Z_2} = \omega_c a^\dagger a + \frac{\omega_a}{2} \sum_{i=1}^N \sigma_i^z + \frac{g}{\sqrt{N}} \sum_{i=1}^N (a^\dagger + a)(\sigma_i^+ + \sigma_i^-) \quad (20)$$

In the frame rotating with the pumping frequency ω_p , the two photon Raman process in the experimental set-up Fig.3a leads to:

$$H_{RS} = \delta a^\dagger a + \int dx dz \Psi^\dagger(x, z) \left[\frac{p_x^2 + p_z^2}{2m} + \frac{\Omega^2}{\Delta_a} \cos^2 kz \right. \\ \left. + \frac{g_0 \Omega}{\Delta_a} (a^\dagger + a) \cos kz \cos kz + \frac{g_0^2}{\Delta_a} \cos^2 kz a^\dagger a \right] \Psi(x, z) \quad (21)$$

where $\delta = \omega_p - \omega_c$, $\Delta_a = \omega_p - \omega_a$. The Z_2 symmetry is $a \rightarrow -a$, $kx \rightarrow kx + \pi$ or $a \rightarrow -a$, $kz \rightarrow kz + \pi$.

At the mean field level, in the two modes approximation, one can decompose the atom field into the superpositions of two momentum (orbital) levels:

$$\Psi_{RS}(x, z) = c_0 \psi_0 + c_1 \cos kz \cos kz \psi_0 \quad (22)$$

where the ψ_0 is the zero crystal momentum state of the lowest Bloch band of the one dimensional Hamiltonian $H_{1d} = \frac{p_z^2}{2m} + \frac{\Omega^2}{\Delta_a} \cos^2 kz$ and $c_0^\dagger c_0 + c_1^\dagger c_1 = N$. Under the Z_2 transformation, $c_1 \rightarrow -c_1$. When comparing Eqn.22 with Eqns.1,19, noting that $\lambda_p = 2\pi/k$, $\lambda = \lambda_p/2 = \pi/k$ in the Fig.3, one can see that the c_1 term corresponds to $P = 4$ with the ordering wavevectors $\vec{G} = (\pm\pi, \pm\pi)$.

Substituting Eqn.22 into Eqn.21 leads to the interacting Hamiltonian between the photon and the effective two momentum (orbital) levels:

$$H_{J-Z_2} = \omega_c a^\dagger a + \omega_a J^z + \tilde{g}(a^\dagger + a)(J^- + J^+) \quad (23)$$

where $\omega_c = \delta - N \frac{g_0^2}{2\Delta_a}$, $\omega_a = 2\omega_r$ where $\omega_r = \hbar^2 k^2 / 2m$ is the recoil energy. The effective interaction is $\tilde{g} = \frac{g_0 \Omega}{\Delta_a}$ and $J^z = \frac{1}{2}(c_1^\dagger c_1 - c_0^\dagger c_0)$, $J^+ = c_0^\dagger c_1$, $J^- = c_1^\dagger c_0$. One can identify Eqn.23 with Eqn.20 after identifying the collective spin operators of the N atoms as $J^z = \frac{1}{2} \sum_{i=1}^N \sigma_i^z$, $J^+ = \sum_{i=1}^N \sigma_i^+$, $J^- = \sum_{i=1}^N \sigma_i^-$.

From Eqn.22, one can see the boson density:

$$n_{RS}(x, z) = \langle c_0^\dagger c_0 \rangle |\psi_0|^2 + \langle c_1^\dagger c_1 \rangle \cos^2 kz \cos^2 kz |\psi_0|^2 + \langle J^x \rangle \cos kz \cos kz |\psi_0|^2 \quad (24)$$

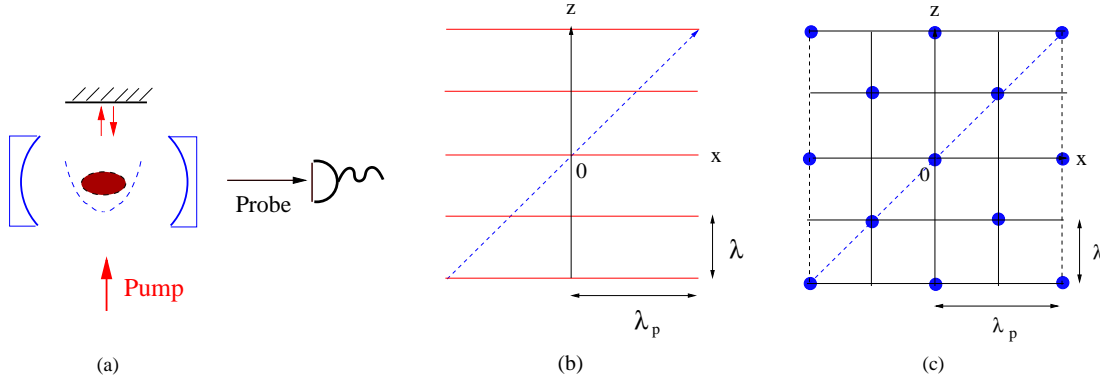


FIG. 3: (Color figure online) (a) Reflected Transverse pumping plus the Standing wave cavity to realize the Z_2 Dicke model, the probe detects the Fluorescence spectrum. The atom distributions of the Z_2 Dicke in (b) and (c) can be detected by the absorption imaging. (b) In the normal phase, the atoms just follow the stripes formed by the reflected transverse pumping. The $\lambda_p = 2\pi/k$, $\lambda = \lambda_p/2 = \pi/k$ where the k is the transverse pumping wave number (c) In the Z_2 superradiant phase for photons and the Z_2 supersolid state for atoms, the atoms take the check-board distribution on the optical lattice formed by the cavity photon and the pumping laser.

In the normal phase, $\langle c_1^\dagger c_1 \rangle = 0$ and $\langle J^x \rangle = 0$, the boson density is just $\sim |\psi_0|^2$ shown in Fig.3b. In the Z_2 super-radiant phase, $\langle c_1^\dagger c_1 \rangle > 0$ and $\langle J^x \rangle \neq 0$, the boson density takes the check-board pattern shown in Fig.3c. The corresponding SF to the SFDW transition of the atoms is in the same universality class of the Z_2 superradiance⁵⁶.

Of course, any symmetry breaking only happens in the thermodynamic limit. For a finite system, the symmetry breaking will be restored. The quantum fluctuations (namely, the finite size effects) in the Z_2 Dicke model is exponentially suppressed $\sim e^{-N}$, but still observable at small N . The quantum fluctuations will restore the Z_2 symmetry, so render $\langle J^x \rangle = 0$, but still keep $\langle c_1^\dagger c_1 \rangle > 0$ inside the Z_2 super-radiant phase. They will transform the check-board pattern in Fig.3c to the uniform distribution on the optical lattice formed by the cavity photon and the pumping laser. The transition from the SF to the SFDW becomes a crossover. The detailed study of quantum fluctuations were given in⁵⁶.

V. CONCLUSIONS

In this paper, we provided a unified and global view on the universal properties of various kinds of supersolids such as their trial wavefunctions, symmetry breaking patterns and excitation spectra in various systems. These systems could be continuous systems such as 3d Helium and 2d excitonic semiconductor systems or various lattice systems such as cold atoms with long range interactions loaded on optical lattices. Inside a SS phase in a continuous system, the effective action Eqn.3 controls the quantum fluctuations above the mean field lattice structure of $\delta n(\vec{x})$ and the condensation structure of $\psi(\vec{x})$. The elementary excitations have two longitudinal modes $\omega_{\pm} = v_{\pm} q$ called "supersolidons" shown in Fig.1. The transverse modes in the SS stay the same as those in the Normal solid. The effects of these two supersolidons on the in-elastic X-ray scattering, neutron scattering, acoustic attenuations and specific heat were discussed in¹⁹⁻²¹. Detecting these "supersolidons" by these

experiments could be smoking gun experiments to confirm a supersolid in any continuous systems. For the first time, we constructed an effective Hamiltonian whose ground state is a supersolid. It can be used to derive the supersolidon spectrum in the whole BZ. We also contrasted the wavefunction and the effective Hamiltonian of a supersolid with that of a commensurate solid with local quantum tunneling and exchange processes. We argued that the dipole-dipole interaction in the in-direct excitons in 2d EHBL may favor the formation of a supersolid more than the Van der Waals interactions between 4He atoms.

Then we discussed the supersolids in lattice systems which are much simpler than its continuous counterparts. Much more established theoretical results from spin wave analysis, dual Ginsburg-Landau and QMC are established in lattice supersolid cases. The valence bond supersolid is a new kind of supersolid unique to lattice systems. The elementary excitations in some of these phases were shown in the Fig.2 and can be contrasted to its continuous counterparts shown in Fig.1. Both interstitial or vacancy like supersolids can happen in lattices slightly away from 1/2 fillings in a bipartite lattice or 1/3 fillings in a frustrated lattice. So they can only happen at in-commensurate fillings. In this regard, the lattice supersolids are similar to its continuous counterparts. The CDW-SS could be realized in possible near future experiments with dipolar bosons or ^{52}Cr atoms loaded in various optical lattices.

We also discussed the superfluid density wave (SFDW) in both fermionic and bosonic systems. It has one order parameter $\psi(x)$ as shown in Eqn.19,22, no the underlying normal solid component $\delta n(\vec{x}) = n(\vec{x}) - n_0$ shown in the first equation in Eqn.1. This crucial difference than the supersolids lead to the important fact that the SFDW can form at any densities instead of just slightly away from commensurate fillings for a supersolid. The first example is the inhomogeneous superfluids (FFLO state) in a continuous system. Its excitation spectrum is similar to those shown in Fig.1. So far, there is no clear experimental evidences of FFLO state in condensed matter or cold atom systems yet, but they are still under extensive experimental searches in both communities. The second example is the Z_2 SFDW inside an optical cavity. Its excitation spectrum is similar to those shown in Fig.2. There is clear experimental evidences of such a Z_2 SFDW in cold atoms inside a transversely pumped high finesse cavity shown in Fig.3. We expect SFDW may also be realized in cold spinor atom BEC systems in the presence of strong spin-orbit coupling generated by artificial non-abelian gauge potentials⁵⁷. The spin-orbit coupling may lead to spontaneous translational symmetry breaking, the theory presented in Sect.IV may apply to such a case. We expect theoretical investigations and experimental searches for various kinds of supersolids in various systems are still active underway.

Acknowledgements

Y.C and Q.S.T's research are supported by NSFC-11074004. J. Ye thank A.V. Balatsky for his hospitality during J.Ye's visit at LANL. J. Ye's research is supported by NSF-DMR-1161497, NSFC-11074173, 11174210, Beijing Municipal Commission of Education under grant No.PHR201107121, at KITP is supported in part by the NSF under grant No. PHY-0551164.

¹ A. Andreev and I. Lifshitz, Sov. Phys. JETP **29**, 1107 (1969).

² G. V. Chester, Phys. Rev. A **2**, 256 (1970).

³ A. J. Leggett, Phys. Rev. Lett. **25**, 1543 (1970).

⁴ E. Kim and M. H. W. Chan, *Nature* 427, 225 - 227 (15 Jan 2004), E. Kim and M. H. W. Chan, *Science* 24 September 2004; 305: 1941-1944, A. Clark and M. Chan, *J. Low Temp. Phys.* **138**, 853 (2005), E. Kim, M. H. W. Chan, *Phys. Rev. Lett.* **97**, 115302 (2006).

⁵ A. S. C. Rittner, J. D. Reppey, *Phys. Rev. Lett.* **97**, 165301 (2006).

⁶ J. Day, T. Herman and J. Beamish, *Phys. Rev. Lett.* **95**, 035301 (2005); J. Day, O. Syshchenko, and J. Beamish *Phys. Rev. B* **79**, 214524 (2009), A. Suhel and J. R. Beamish *Phys. Rev. B* **84**, 094512 (2011).

⁷ M. W. Ray and R. B. Hallock, *Phys. Rev. Lett.* **100**, 235301 (2008); *Phys. Rev. B* **79**, 224302 (2009); *Phys. Rev. Lett.* **105**, 145301 (2010); *Phys. Rev. B* **84**, 144512 (2011).

⁸ I. A. Todoshchenko, H. Alles, J. Bueno, H. J. Junes, A. Ya. Parshin, and V. Tsepelin, *Phys. Rev. Lett.* **97**, 165302 (2006); *JETP* **85**, 555 (2007).

⁹ J. M. Goodkind, *Phys. Rev. Lett.* **89**, 095301 (2002); G. Lengua and J. M. Goodkind, *J. Low Temp. Phys.* **79**, 251 (1990)

¹⁰ C.A. Burns and J.M. Goodkind, *J. Low Temp. Phys.* **95**, 695 (1994).

¹¹ E. Blackburn, *et.al*, *Phys. Rev. B* **76**, 024523 (2007)

¹² D. M. Ceperley, B. Bernu, *Phys. Rev. Lett.* **93**, 155303 (2004)

¹³ D. E. Galli, M. Rossi, L. Reatto, *Phys. Rev. B* **71**, 140506(R) (2005); D. E. Galli and L. Reatto, *Phys. Rev. Lett.* **96**, 165301 (2006).

¹⁴ P. W. Anderson, W. F. Brinkman, D. A. Huse, *Science* 18 Nov. 2005; **310**: 1164-1166.

¹⁵ P. W. Anderson, *Science* **324**, 631 (2009).

¹⁶ A. T. Dorsey, P. M. Goldbart, J. Toner, *Phys. Rev. Lett.* **96**, 055301 (2006).

¹⁷ C.-D. Yoo and A. T. Dorsey, *Phys. Rev. B* **81**, 134518 (2010);

¹⁸ D.T. Son, *Phys. Rev. Lett.* **94** (2005) 175301; C. Josserand, Y. Pomeau, and S. Rica, *Phys. Rev. Lett.* **98**, 195301 (2007). See also earlier works, T. Schneider and C.P. Enz, *Phys. Rev. Lett.* **27**, 1186 (1971); Y. Pomeau and S. Rica, **72**, 2426 (1994).

¹⁹ J. Ye, *Phys. Rev. Lett.* **97**, 125302 (2006).

²⁰ J. Ye, *Europhysics Letters*, **82** 16001 (2008)

²¹ J. Ye, *J. Low Temp Phys.* **160**(3), 71-111,(2010)

²² P. Nozieres, *J Low Temp Phys* **156**, 9C21 (2009).

²³ A. V. Balatsky, M. J. Graf, Z. Nussinov and S. A. Trugman, *Phys. Rev. B* **75**, 094201 (2007).

²⁴ L. Modesto, D.L.S. Jnior, J.N. Rabelo, L. Candido, *Solid State Communications* **145**, 355 (2008); A. Stoffel, M. Gulcsi, *Europhysics Letters*, **85**, 20009 (2009); S. Datta, S. Yarlagadda, *Solid State Communications* **150**, 2040 (2010).

²⁵ S. Balibar, F. Caupin, *Journal of Physics, Condensed Matter* **20**, 173201 (2008).

²⁶ G. S. Jeon and J. Ye, *Phys. Rev. B* **71**, 035348 (2005), J. Ye, *Phys. Rev. B* **71**, 125314 (2005), L. Jiang and J. Ye, *Phys. Rev. B* **74**, 245311 (2006), J. Ye, *Annals of Physics*, **323** (2008), 580-630.

²⁷ For example, see the appendix N of *Solid State Physics*, N. W. Ashcroft and N. D. Mermin, 1976.

²⁸ The fact that the superfluid density is proportional to the vacancy density is similar to the Uemura relation in high T_c superconductors. See for example, J. Ye and S. Sachdev, *Phys. Rev. B* **44**, 10173 (1991).

²⁹ J. Ye, *J. Low Temp Phys.* **158**(5), 882-900 (2010).

³⁰ L. Balents *et al*, *Phys. Rev. B* **71**, 144508 (2005).

³¹ L. Jiang and J. Ye, *J. Phys. Condensed Matter.* **18** (2006) 6907-6922

³² J. Ye, *Nucl. Phys.B* **805** (3) 418-440 (2008).

³³ Y. Chen and J. Ye, arXiv:0804.3429, v3, to appear in *Philosophical Magazine*.

³⁴ Y. Chen and J. Ye, arXiv:0612009, v4. To appear in Nucl. Phys. B.

³⁵ A. W. Sandvik, Phys. Rev. Lett. 98, 227202 (2007).

³⁶ One can understand these results from Fig.2 intuitively. (1) From Right to the middle in Fig.2, across the transition from the CDW (VBS) to the CDW-SS (VB-SS), the CDW (VBS) mode has a gap across the transition, so can be integrated out, the SF mode is the only low energy mode, so the CDW to the CDW-SS transition is in the same universality class of the Mott to SF transition. (2) From left to the middle in Fig.2, across the transition from the SF_1 (SF_2) to the CDW-SS (VB-SS), there are SF modes on both sides, so they may couple to possible critical density fluctuation mode near the transition, so the nature of the transition is much more complicated, may be resolved by high precision QMC on specific microscopic models. For example, the $V_1 > 0, V_2 > 0$ model Eqn.17 in Sec.III-B-1 may be in a different universality class than the dipole-dipole intercation model in Sec.III-B-2.

³⁷ G. Murthy, D. Arovas, A. Auerbach , Phys. Rev. B 55, 3104-3121 (1997).

³⁸ F. Hebert *et.al*, Phys. Rev. B 65, 014513 (2001)

³⁹ P. Sengupta, *et.al*, Phys. Rev. Lett. 94, 207202 (2005).

⁴⁰ J. Y. Gan, *et.al* Phys. Rev. B 75, 214509 (2007).

⁴¹ G.G. Batrouni, *et.al* Phys. Rev. Lett. 97, 087209 (2006), Phys Rev A72, 031601(R) (2005).

⁴² D. Heidarian and K. Damle, Phys. Rev. Lett. **95**, 127206 (2005); S. Wessel and M. Troyer, Phys. Rev. Lett. **95**, 127205 (2005).

⁴³ S. V. Isakov, *et al*, Phys. Rev. Lett. 97, 147202 (2006); K. Damle and T. Senthil, Phys. Rev. Lett. 97, 067202 (2006).

⁴⁴ K.-K. Ni, *et al*, Science 322, 231 (2008).

⁴⁵ B. C. Sansone, *et al*, Phys. Rev. Lett. 104, 125301 (2010). It seems there is a factor of $1/N$ missing in the structure factor defined in this paper.

⁴⁶ L. Pollet, J. D. Picon, H. P. Bkhler, and M. Troyer, Phys. Rev. Lett. 104, 125302 (2010).

⁴⁷ J. R. Armstrong, N. T. Zinner, D. V. Fedorov and A. S. Jensen, EPL 91 16001 (2010).

⁴⁸ A. Griesmaier, *et.al*, Phys. Rev. Lett. 94, 160401 (2005)

⁴⁹ J. Ye, *et al*, Phys. Rev. A 83, 051604 (R) (2011).

⁵⁰ J. Ye, *et al*, arXiv:0812.4077, v5, to appear in Annals of Physics.

⁵¹ P. Fulde and R. A. Ferrell, Phys. Rev. 135, A550-563 (1964).

⁵² A. I. Larkin and Yu. N. Ovchinnikov, Sov. Phys. JETP 20, 762(1965)

⁵³ L. Jiang and J. Ye, Phys. Rev. B 76, 184104 (2007).

⁵⁴ A. T. Black, H. W. Chan and V. Vuletic, Phys. Rev. Lett. 91, 203001(2003).

⁵⁵ K. Baumann, *et.al*, Nature 464, 1301-1306 (2010).

⁵⁶ For the $U(1)$ Dicke (Tavis-Cummings) model, see J. Ye and C. Zhang, Phys. Rev. A 84, 023840 (2011), For the Z_2 Dicke model, see Y. Chen, J. Ye *et al*, preprint.

⁵⁷ J. Dalibard, F. Gerbier, G. Juzelinas, P. Ohberg, Rev. of Mod. Phys. 83, 1523 (2011).